3 Harmonic Tremor: Analysis

As other volcanic seismic signals, harmonic tremor at Lascar must be generated by some physical or chemical process in the volcano. What and where is its source? How are the seismic waves generated by the source affected by their path through the volcano? What does it tell us about the physics of volcanoes? Because the Lascar recordings have a high signal-to-noise ratio, they can be analyzed using standard seismological methods, as well as methods from other fields. The results of this analysis may then serve as the basis for a physical model for the source of harmonic tremor.

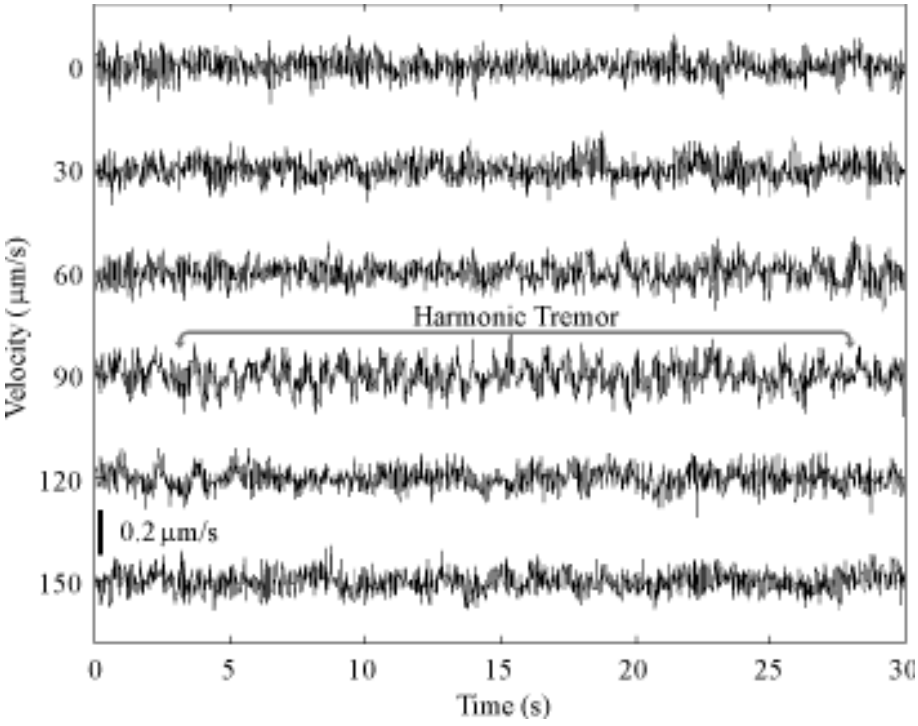

Figure 3.1 Beginning of harmonic tremor. 180 s of the recording of the E component at station LA2 are plotted like a helicorder record. In the 25 s long segment beginning at second 93 which is marked by a bracket, there is a hint of an 0.7 Hz oscillation which differs from the surrounding noise. The interval begins on 18 April 1994 at 01:36:00 UTC. The bar on the lower left shows the amplitude scale.

3.1 Seismograms

3.1.1 Waveforms

At its beginning, harmonic tremor slowly rises above the normal seismic noise signal (Figure 3.1). As is the case with other types of tremor, there is no clear onset. In the

marked segment at 93 s, an oscillation is apparent which differs from the usual noise and lasts about 25 s. About 19 min later, the cycles which are harmonic tremor become clearly recognizable in the seismogram (Figure 3.2).

The cycles of the harmonic tremor can be seen clearly on all stations and components of the Lascar network (Figure 2.11). The period of the cycles is the same at all stations, only the signal shape varies from station to station and component to component.

3.1.2 Amplitudes

AKI and RICHARDS [1980] give the following relationship between the *i*th component of the displacement wavefield for body waves, $u_i(\mathbf{x},t)$, and a point force in the j direction, $F_0(t)$, if the medium is elastic and there is neither scattering nor absorption:

$$u_i(\mathbf{x},t) = \frac{1}{4\pi\rho}(3\gamma_i\gamma_j - \delta_{ij})\frac{1}{r^3}\int_{r/\alpha}^{r/\beta}\tau F_0(t-\tau)d\tau + \frac{1}{4\pi\rho\alpha^2}\gamma_i\gamma_j\frac{1}{r}$$
$$-\frac{1}{4\pi\rho\beta^2}(\gamma_i\gamma_j - \delta_{ij})\frac{1}{r}F_0(t - r/\beta) \qquad (3.1)$$

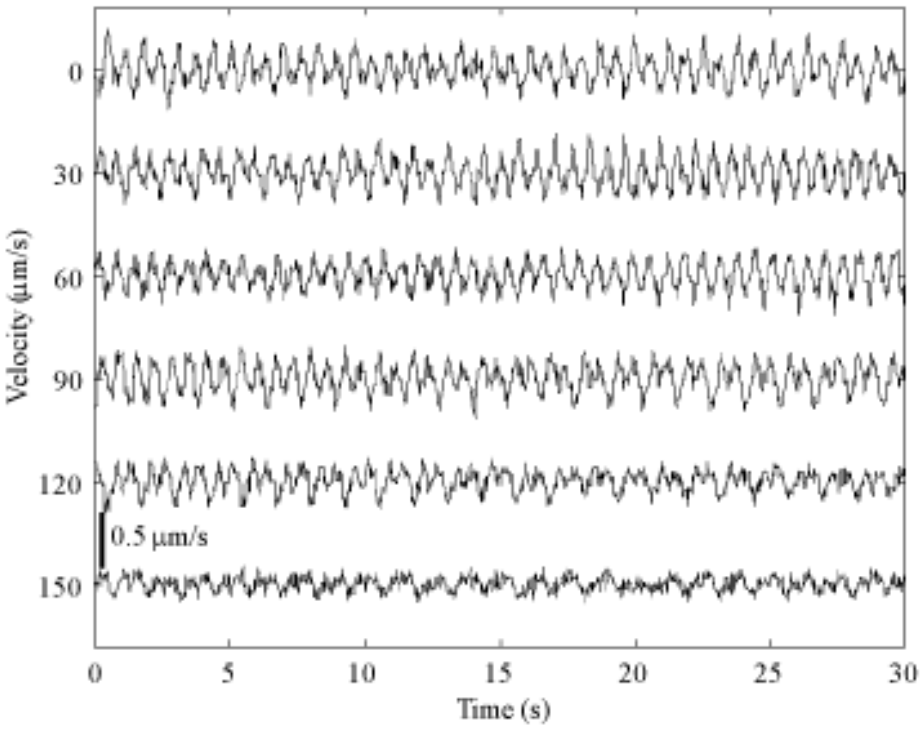

Figure 3.2 Typical 180 s long segment of harmonic Tremor on the recordings of the E component at station LA2. This interval begins at 01:55:00 UTC on 18 April 1994. The bar on the lower left shows the amplitude scale.

In this equation, γ_i and γ_j are the directional cosines and δ_{ij} is the Kronecker delta function, while ρ, α and β are the density of the medium and its P and S wave velocities, respectively. The first term decreases in amplitude with $1/r^3$, so it gives the displacement in the near field. The second and third terms describe the far-field ground motion due to the P and S waves, respectively.

For harmonic tremor, the peak-to-peak ground velocity is about 4×10^{-7} m/s at the station closest to the active crater, LA2, and lower at the other, more distant stations (Figure 2.11). The peak-to-peak ground displacement at station LA2 is about 6×10^{-8} m. This value can be used in Equation 3.1 to estimate the amplitude of a point force at the origin. For this calculation, I assume that the medium has the density of andesite, $\rho = 2.8 \times 10^3$ kg/m^3 [MURASE and MCBIRNEY, 1973], and that the factors containing the directional cosines have their maximum value, γ_i, γ_j =1. For each station, r is taken to be the horizontal distance from the crater to the station. If the wavefield at the station consists

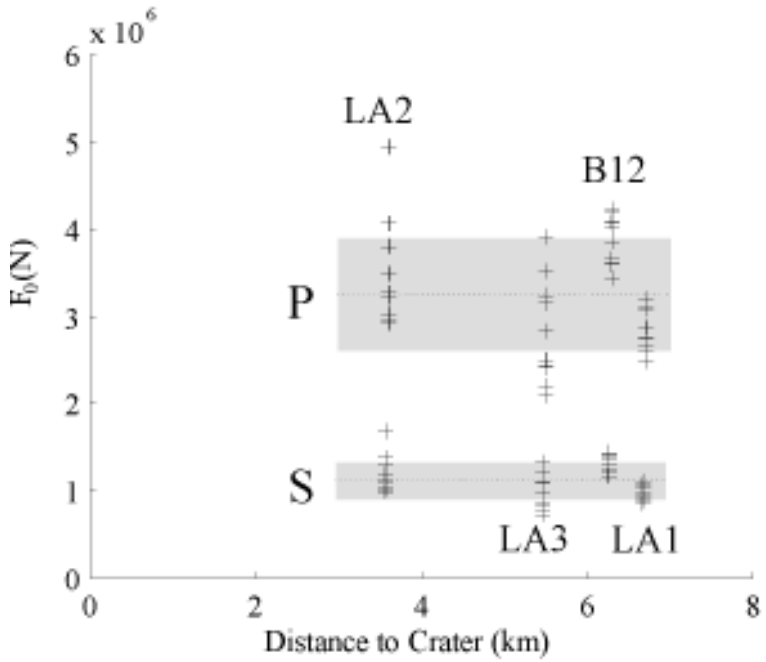

Figure 3.3 Magnitude of a point force necessary to generate recorded seismograms for P and S waves. The force is calculated from 40 s windows of the 400 s interval starting at 02:38:20 UTC on 18 April 1994 using Eq. 3.1. The dotted lines indicate the means, and the vertical extent of the shaded rectangles give the standard deviations.

only of P waves in the farfield, propagating at a velocity α = 1000 m/s, the force necessary to generate the ground displacement due to harmonic tremor at the stations can be estimated using the second term in Equation 3.1. Mean values for F_{0P}, calculated for 40 s windows of data, are plotted in Figure 3.3 for each station along with their average $F_{0P} = 3.2\text{x}10^6$ N. This figure also shows the values of F_{0S} for a wavefield of S waves (β = 580 m/s). In this case, the force at the origin is smaller, $F_{0S} = 1.1\text{x}10^6$ N. Variations in the velocity of the medium or near-field effects may increase the estimated amplitude of the force. On the other hand, contributions from other factors, such as greater source depth or absorption in the medium, would cause the amplitude to decay more rapidly with distance than described by Equation 3.1. The source would then have to produce more seismic energy to generate the measured ground motion.

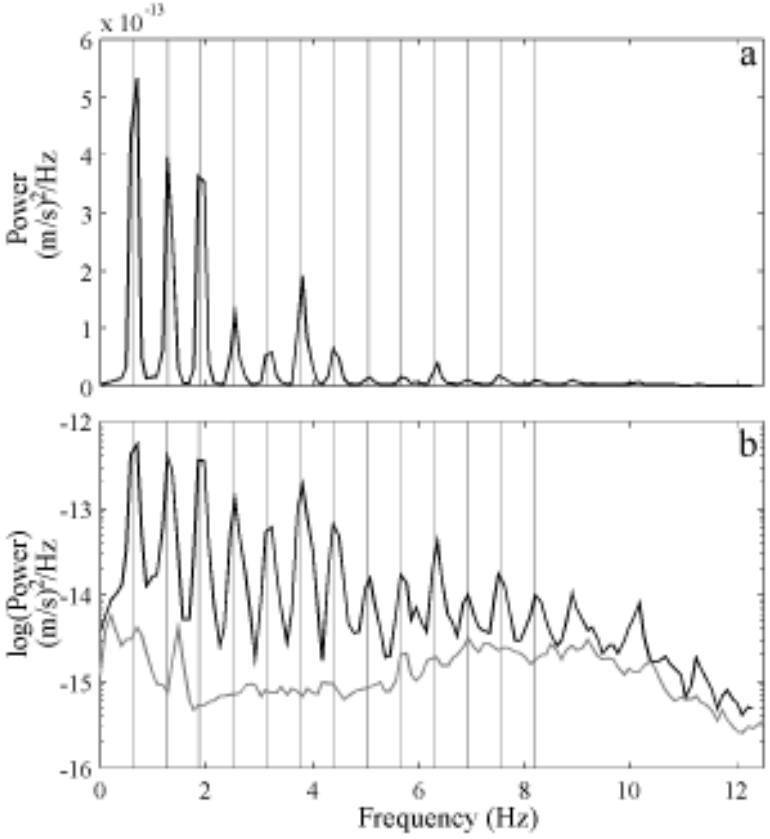

Figure 3.4 Power spectrum of a 10 minute interval of harmonic tremor beginning on 18 April 1994 at 02:35:00 UTC recorded on the E component of station LA2. The spectrum was calculated using 10.24 s windows and 50% overlapping. The vertical lines are drawn at multiples of the frequency of the first peak, 0.63 Hz. (a) Linear plot. (b) Semilog representations. The gray line shows the power spectrum for the 10 minute seismogram segment just before harmonic tremor begins (01:30 UTC).

3.2 Spectra and Spectrograms

3.2.1 Powerspectra

In a linear representation of the power spectrum of harmonic tremor (Figure 3.4a), seven spectral peaks are visible. The frequencies of these peaks are integer multiples of the frequency of the fundamental, f_1 = 0.63 Hz. Spectral peaks of order higher than seven which are only hinted at in Figure 3.4a are visible in the logarithmic representation in Figure 3.4b. Here at least 14 peaks are present which can be described by the equation $f_n = nf_1$. In Figure 3.4b the power spectrum of the background tremor shortly before the beginning harmonic tremor is also plotted (gray). Its spectrum is everywhere lower than

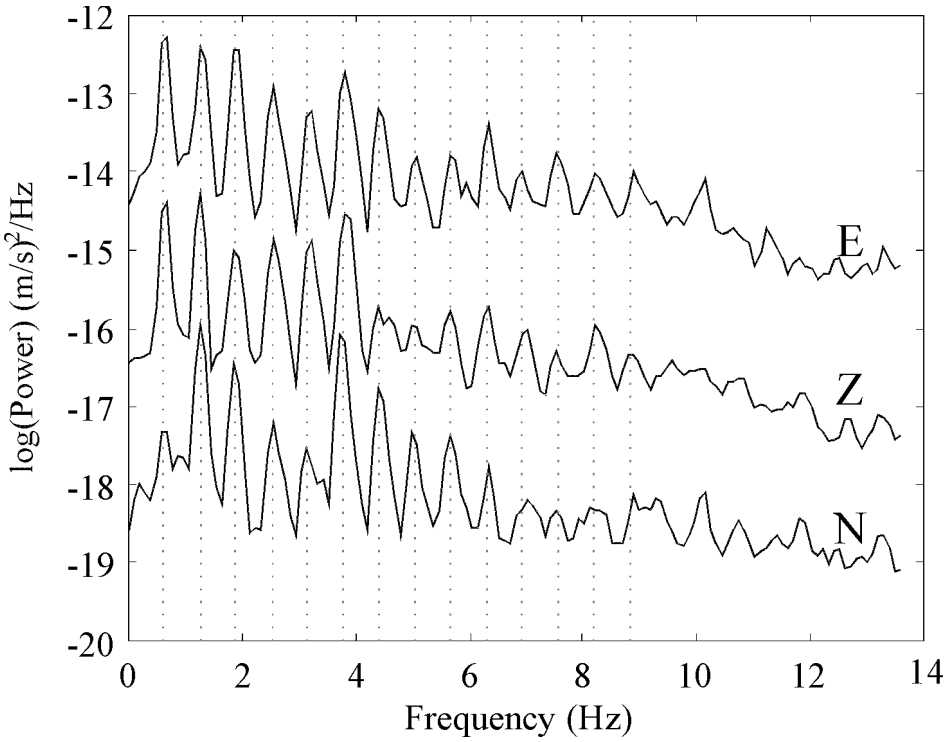

Figure 3.5 Semilog plot of power spectra calculated for the three components of station LA2. The data interval, windows and overlap are the same as Figure 3.4. Spectra for the Z and N components are offset by two and four orders of magnitude to improve viewing. The vertical lines are drawn at multiples of the frequency of the first peak, 0.63 Hz.

the spectrum of the harmonic tremor and it has none of the spectral peaks present in the harmonic tremor.

The logarithmic representation of the power spectra for the three components of station LA2 demonstrates that the Z, N and E components measure signals with the same frequencies but very different amplitudes (Figure 3.5). The same spectral lines are also present in the seismograms recorded at the other stations (Figure 3.6). At all stations the lines up to order seven are between 10 and 20 dB above the noise level. Spectral lines of higher order are only 5 dB above the noise with still lower amplitudes at the more distant stations, LA1 and LA3.

3.2.2 Spectrograms

Spectra (Figures 3.4, 3.5 and 3.6) can only show average values of a signal's ampitude, because they are calculated for an interval of a time series, rather than an instant. In addition, power spectra are usually calculated by averaging over several individual spectra.

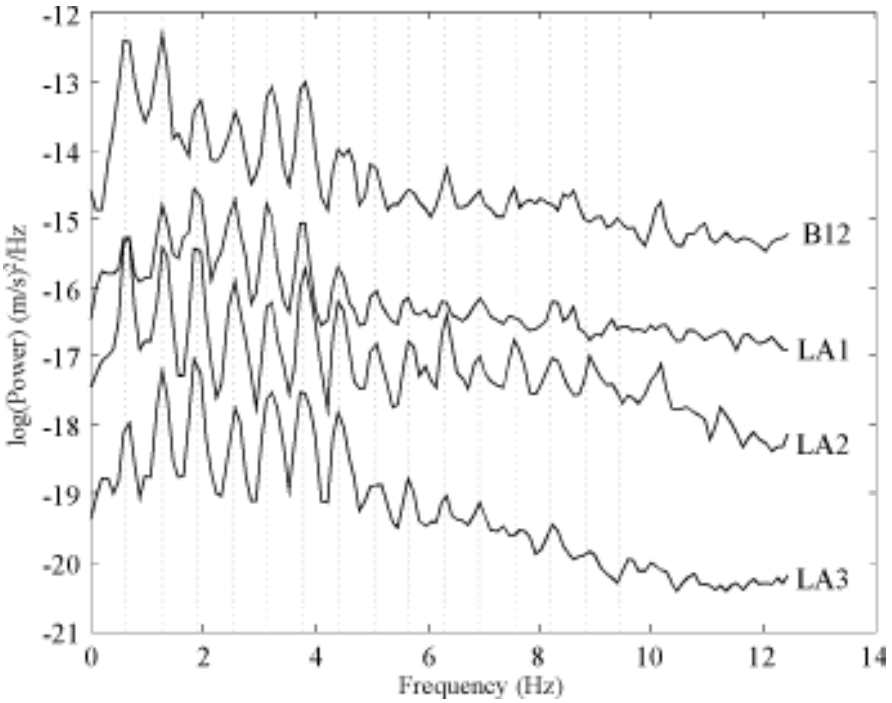

Figure 3.6 Semilog plot of power spectra calculated for the E components of all stations. The data interval, windows and overlap are the same as Figure 3.4. Spectra of LA1, LA2 and LA3 are shifted vertically to improve viewing. The vertical lines are drawn at multiples of the frequency of the first peak, 0.63 Hz.

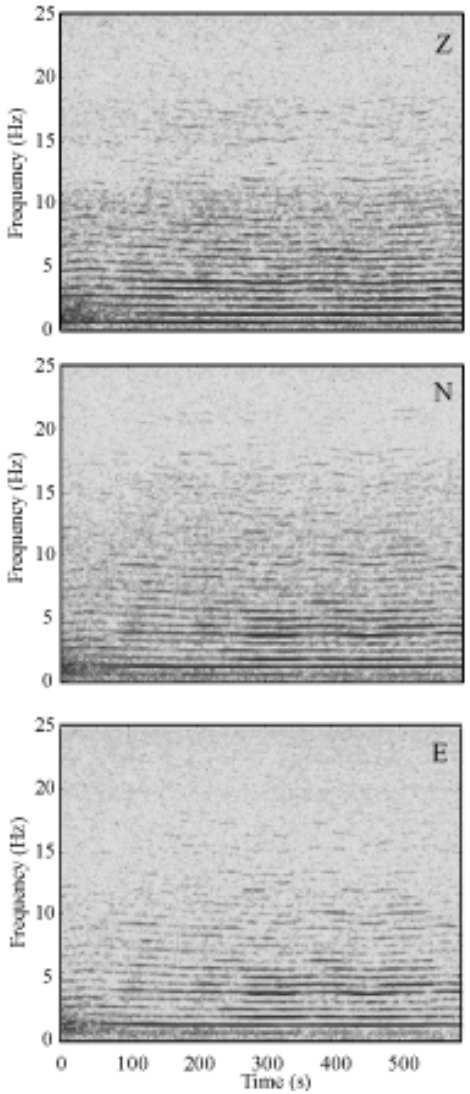

Figure 3.7 Spectrograms of data recorded on the Z, N and E components at station LA2 for the interval used in Figure 3.4. Each spectral window is 10.24 s long, and overlapped by 8.96 s.

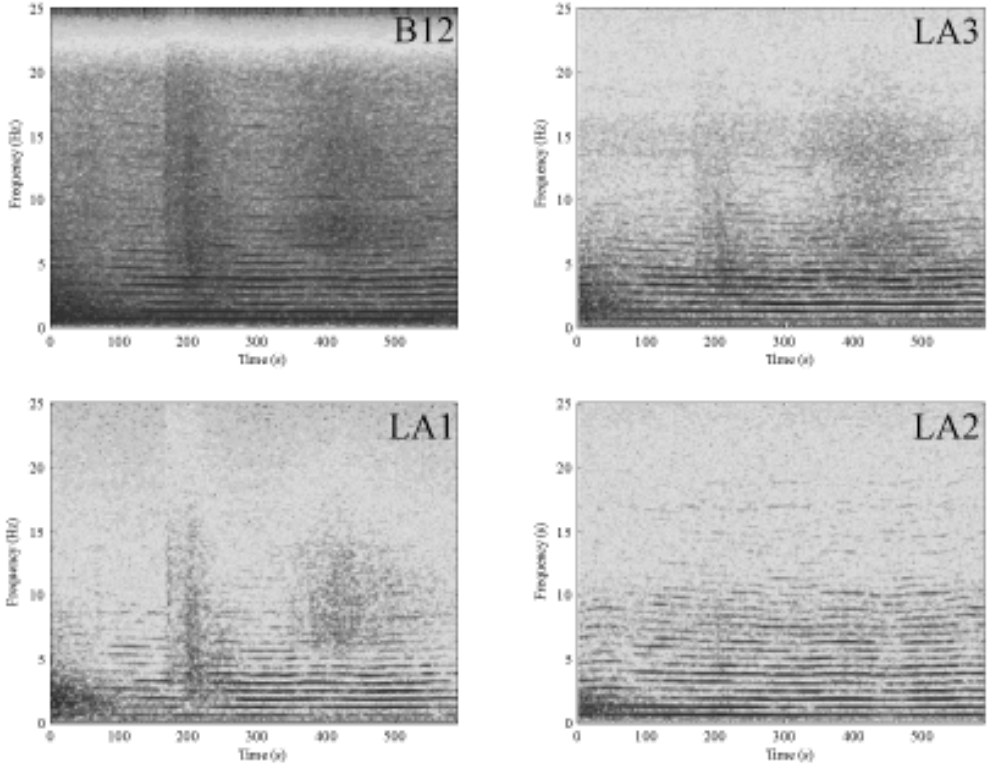

Figure 3.8 Spectrograms of the E components of all four stations of the Lascar network for the interval used in Figure 3.4. They were calculated in the same way as Figure 3.7.

In the analysis of tremor which continues for long periods of time, it is desirable to be able to observe changes in the spectrum as a function of time. Spectrograms allow the representation of the time-dependence of the frequency of a signal. In such plots, the spectral amplitude is usually indicated by color or shading. In a spectrogram representation of the harmonic tremor at Lascar (Figure 2.12), frequency changes are recognizable at 3000 s, 5800 s and 6500 s. At the station nearest to Lascar's crater, LA2, the spectrograms of the components (Figure 3.7) show more than 25 harmonics. The frequency characteristics of the tremor can be recognized on all components (Figure 3.7) and at all stations (Figure 3.8). Changes in the frequency observed at Station LA2 occur at the same time at the other stations. This observation leads to the conclusion that such changes are produced at the source and are not caused by characteristics of the path or station site.

3.2.3 Phasorgrams

Volcanic tremor can be distinguished from seismic events by the fact that its source or sources are continuously active over long periods of time. Thus, it makes little sense to search a tremor recording for the changes in amplitude and and frequency that signal the arrival of seismic phases. On the other hand, the presence and behavior of narrowband signals in tremor can be resolved using complex demodulation.

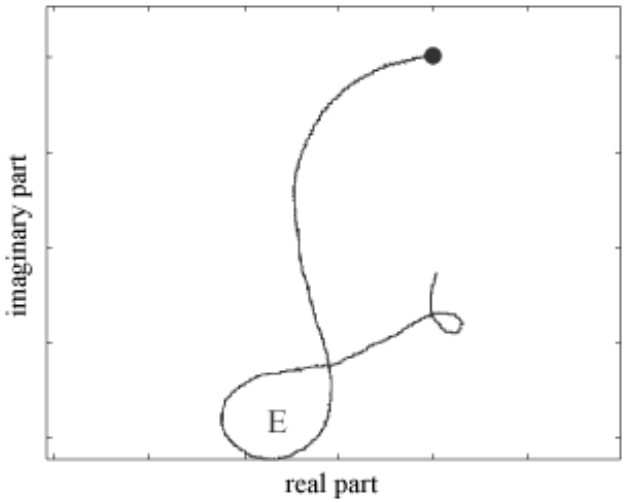

Figure 3.9 Phasorgram for the fundamental recorded on the E component at station LA2. The test frequency is f_0 = 0.63 Hz. A bandpass filter with corner frequencies at 0.5 and 0.9 Hz was applied to the data be fore the phasorgram was calculated. t = 0 is indicated by the dot.

In the method of “phasor walk-outs” — or phasorgrams — described by ZÜRN and RYDELEK [1994], the Fourier transform $X(f_0,n)$ of a time series $x(k\Delta t)$ is calculated not, as is usual, for all frequencies f, but only for a “test frequency” f_0,

$$X(f_0,n) = C\sum_{k=1}^{n} x(k\Delta t)\cdot e^{-2\pi i f_0 k\Delta t}, \qquad (3.2)$$

where C is a scaling factor. The complex function $X(f_0,n)$ is then plotted in the complex plane. In the resulting diagram, very weak, narrowband signals at or near the test frequency can be recognized, as well as changes in the frequency of the signal or phase jumps [ZÜRN and RYDELEK, 1994]. The radius of curvature is an indication for the difference between the test frequency and the frequency of the signal. As a general rule, the smaller the radius of curvature, the farther the signal frequency is from the test frequency.

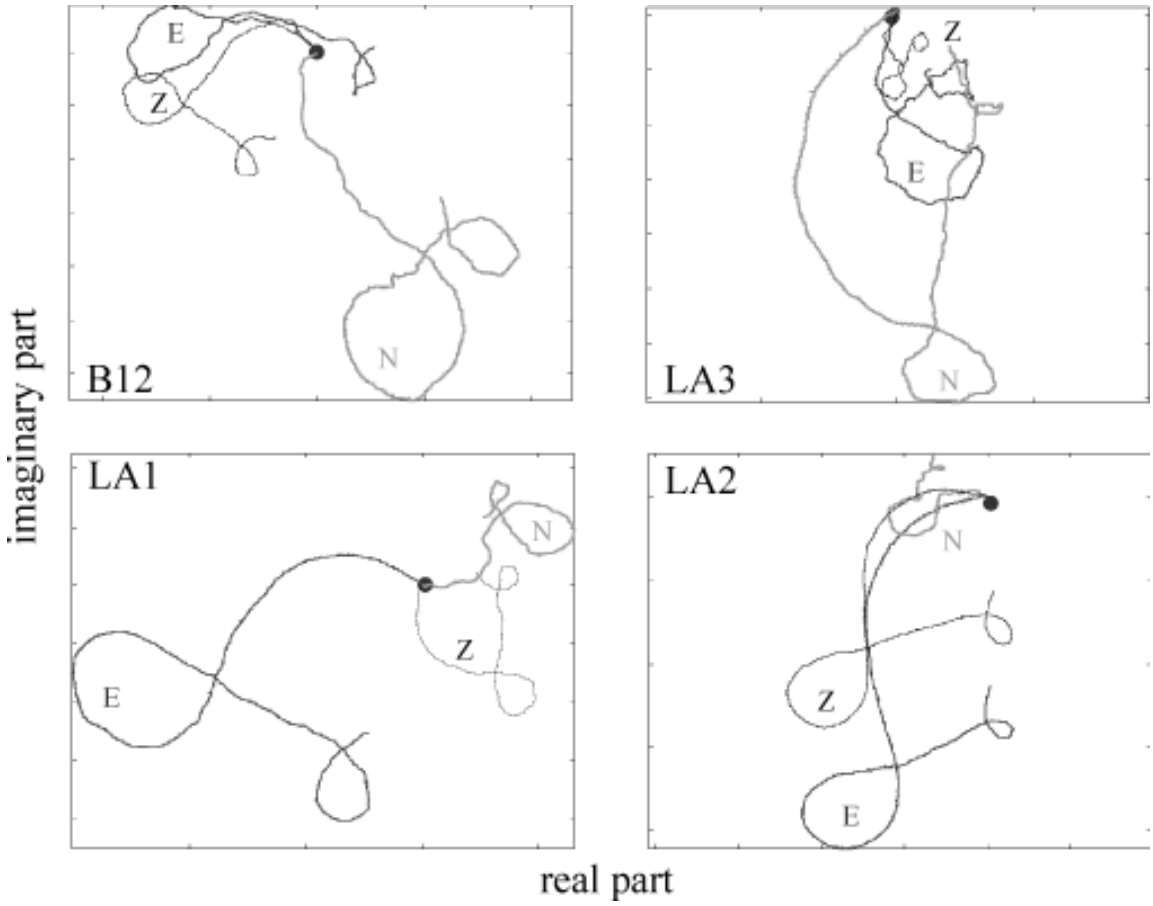

Figure 3.10 Phasorgram as in Figure 3.9 for all components at all stations. $t = 0$ is indicated by the dot.

As an example, I calculate the phasorgram for a 2 minute interval of the bandpass filtered data (0.5-0.9 Hz) for the E component at station LA2 (Figure 3.9). The test frequency, f_0 = 0.63 Hz, corresponds to the maximum of the peak for the fundamental in the power spectrum. The variation in the radius of curvature of the phasorgram curve shows the deviation of the frequency of the tremor from the test frequency. The curve begins with a large arc, indicating that the tremor frequency is close to f_0. The next segment is nearly straight, so the tremor frequency is exactly 0.63 Hz. In the following section (around the letter E), the radius of curvature is much smaller than for the first interval. At the end of the phasorgram another straight segment is followed by a very small loop, where the tremor frequency has drifted quite far from the test frequency. As indicated by these plots, the tremor frequency varies continuously and smoothly.

The individual phasorgrams for the three components at the station LA2 (Figure 3.10, lower right) all show similar pattern of loops and straight segments, although their directions and amplitudes differ. This is not surprising, since the seismometer partitions the ground motion into three orthogonal directions which are arbitrarily related to the polarization of the oscillations. On the other hand, the phasorgrams at the other three stations are very similar to those at station LA2 (Figure 3.10). Although the polarizations of the oscillations at the four stations appear to be unrelated to each other (see section 3.4), the phasorgrams have the same pattern with an arc, followed by a straight section, a large loop, another straight section and finally a small loop. This similarity means that the frequency changes of harmonic tremor are independent of path and site.

3.3 The Reduced Instantaneous Phase

The Hilbert transform of a real function of time $x(t)$ is:

$$y(t) = \mathrm{H}(x(t)) = \tfrac{1}{\pi} P \int_{-\infty}^{\infty} \frac{x(\xi)}{\xi - t} d\xi \,, \qquad (3.3)$$

where, ξ is the variable of integration for the time and P is the principal value of the integral [Buttkus, 1991]. Adding this function to the original function as the imaginary part gives the

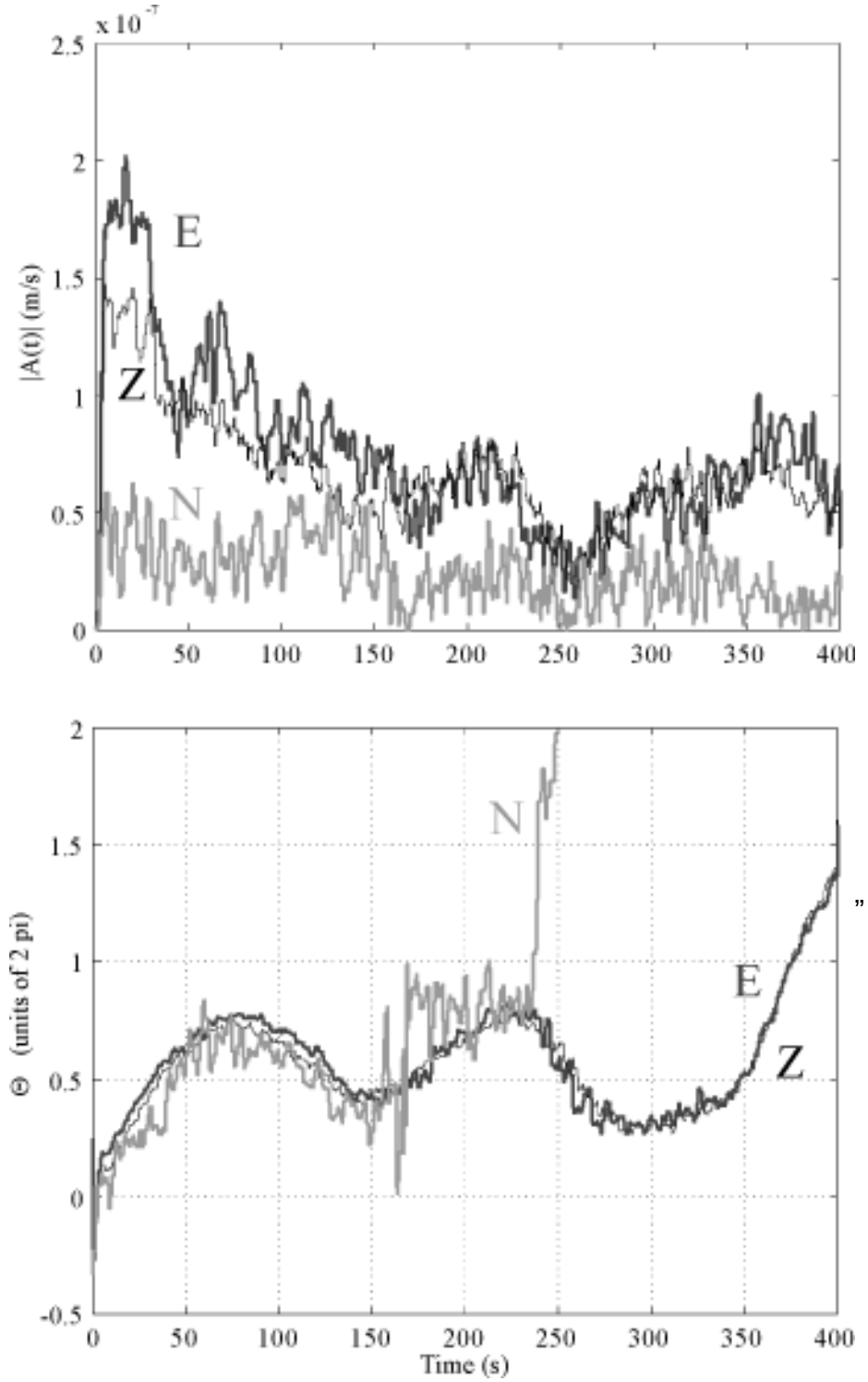

Figure 3.11 Hilbert transform of the fundamental at station LA2. Top: The instantaneous amplitude. Bottom: The reduced instantaneous phase Θ_R with f_0 = 0.63. A bandpass filter with corner frequencies at 0.5 and 0.9 Hz was applied to the data before the Hilbert transform was calculated. The data interval begins at 02:38:20 UTC on 18 April 1994.

analytic function, $z(t)$, which can also be expressed in terms of the instantaneous amplitude, $A(t)$, and the instantaneous phase, $\Theta(t)$:

$$z(t) = x(t) - i\mathrm{H}(x(t)) = x(t) - iy(t) = A(t)e^{i\Theta(t)}. \quad (3.4)$$

In seismology this function may be used to determine the group and phase velocities of surface waves [DZIEWONSKI and HALES, 1972]. The Hilbert transform has also been applied to seismological data to determine arrival times and polarization (FARNBACH, 1975, VIDALE, 1986).

The time derivative of the instantaneous phase is the instantaneous angular frequency:

$$\omega(t) = 2\pi f(t) = \frac{d\Theta(t)}{dt}. \quad (3.5)$$

If $x(t)$ is a sine wave, $x(t)=\sin(2\pi f_0 t)$, then its Hilbert transform is $y(t)=\cos(2\pi f_0 t)$ and its instantaneous phase is a straight line with slope $2\pi f_0$. For narrowband signals we can use this fact to detect and measure even very small changes in the frequency. Let $s(t)$ be a recorded, sinusoidal signal with time varying amplitude, $A_1(t)$, and slowly changing frequency, $f(t)$,

$$s(t) = A_1(t)\sin(2\pi f(t)t). \quad (3.6)$$

If the changes of $f(t)$ around some value f_0 are small, they can be measured by plotting the reduced instantaneous phase ,

$$\Theta_R = \Theta(t) - 2\pi f_0 t, \quad (3.7)$$

as a function of time. When $f(t)= f_0$, the slope of Θ_R,

$$m = 2\pi(f(t)- f_0), \quad (3.8)$$

will be zero. During intervals when $f(t)$ is constant, m is constant, and the slope of the reduced instantaneous phase changes when $f(t)$ changes.

While the phasorgrams described in Section 3.2.3 allow the qualitative analysis of the variations in the tremor frequency, the analytic function permits quantitative observations of

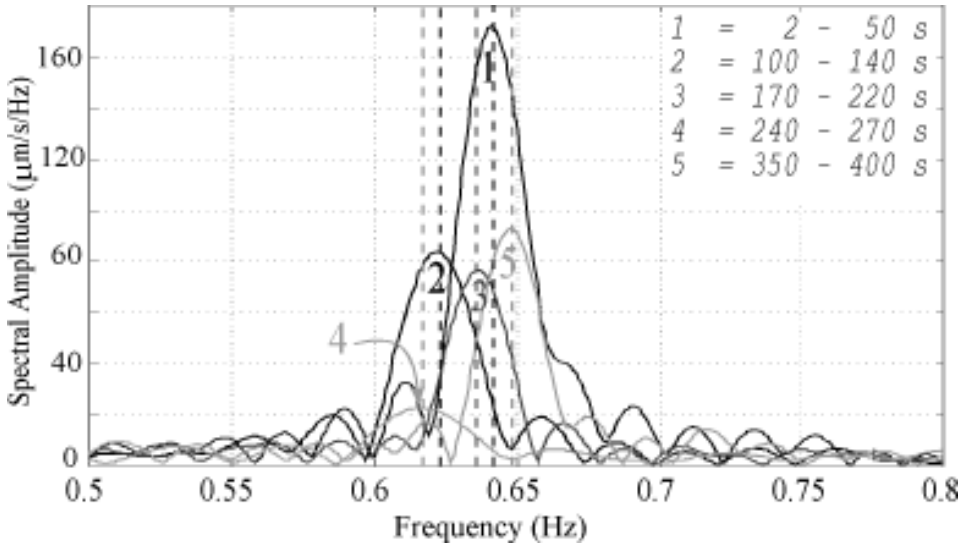

Figure 3.12 Determination of the exact frequency of the fundamental from the amplitude spectrum in five intervals. Before the spectra were calculated, zeros were appended to the data from each interval so that they were 50000 values long. The frequency separation of the spectral values is then 0.001 Hz. The vertical lines show the frequencies measured using the Θ_R.

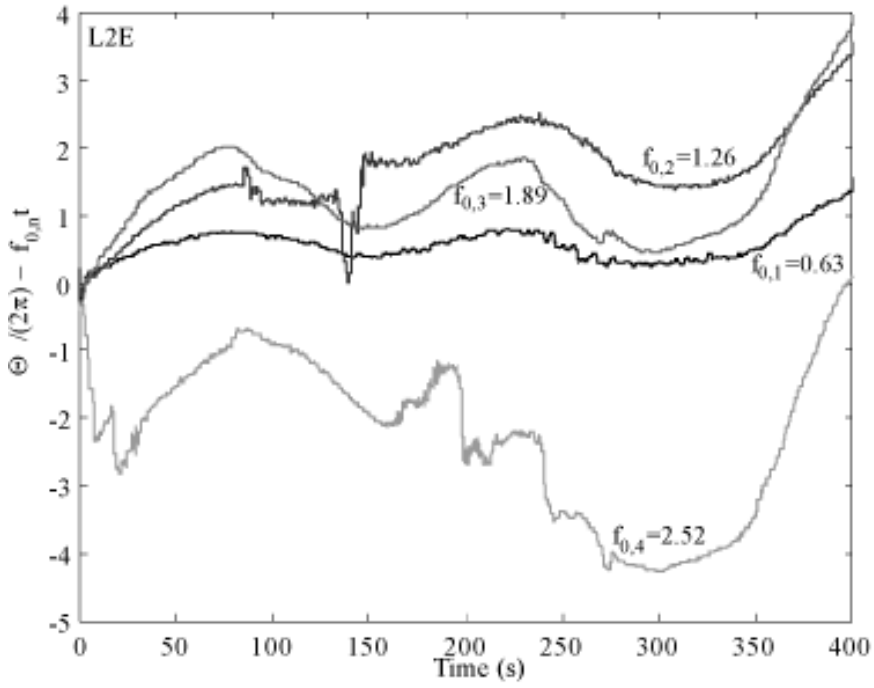

Figure 3.13 Comparison of the Θ_R for the first four harmonics at station LA2. Before calculating Θ_R, bandpass filters were applied to the data. The corner frequencies are: n =1, 0.5-0.9 Hz; n =2, 0.9-1.5 Hz; n =3, 1.5-2.1 Hz; n =4, 2.1-2.7 Hz. The test frequencies for each harmonic are given on the plot. The data interval begins at 02:38:20 UTC on 18 April 1994.

its changes. This is demonstrated in Figure 3.11 where the instantaneous amplitude (top) and Θ_R (bottom) are plotted for 400 s of the recording of the fundamental (bandpass filter 0.5-0.9 Hz) at LA2. Apart from very small variations, Θ_R for the Z and E components are the same. During the first 150 s, the N component is also similar to the other two components. It varies somewhat more because the signal-to-noise ratio (SNR) is much poorer than for Z and E. At 170 s the N component has several jumps of 2π. Here the SNR is low, so the instantaneous phase, $\Theta(t)$ is poorly defined. After a jump of 2π, the phase indicates the same location in the complex plane, so for the analysis of the reduced instantaneous phase, such jumps are of no consequence. Finally, after 240 s, the amplitude of the N component is so small that there are many jumps of 2π and the reduced instantaneous phase wanders out of the range of the figure.

For a quantitative analysis of the reduced instantaneous phase for the Z and E components, the curve in Figure 3.11 can be separated into five segments with relatively constant slope (2<t<50 s, 100<t<140 s, 170<t<220 s, 240<t<270 s and 350<t<400 s). Between these segments the slope changes radically. Using equation 3.8 I can calculate the deviation of the frequency of the fundamental from the test frequency, f_0 = 0.63 Hz. Table 2 gives the results with an accuracy of 0.001 Hz. The frequency for these intervals can also be measured from the maximum of the peak in the amplitude spectrum. In order to achieve an accuracy similar to that determined from Θ_R, the intervals had to be extended to 50000 data points (Figure 3.12). The frequencies, f_S, measured from the spectra agree very well with those determined by the analysis of Θ_R (Table 2).

Table 2 -- Tremor Frequency

Interval	Slope (1/s)	f_1 (Hz)	f_s (Hz)
2-50 s	0.0117 ± 0.0001	0.642	0.641
100-140 s	-0.0069 ± 0.0005	0.623	0.622
170-220 s	0.0065 ± 0.0004	0.636	0.636
240-270 s	-0.0108 ± 0.0023	0.617	0.617
350-400 s	0.0180 ± 0.0007	0.648	0.648

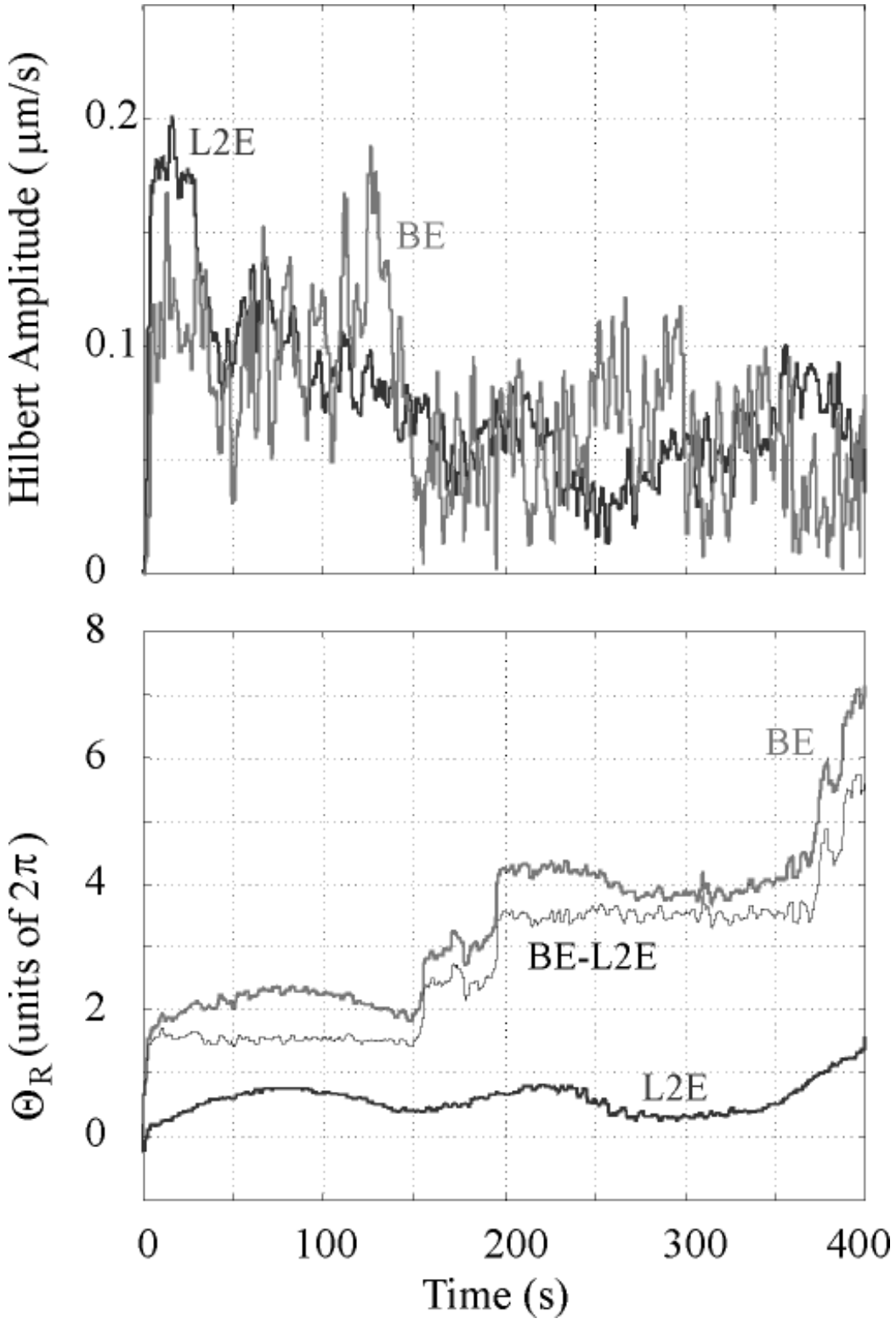

Figure 3.14 Comparison of the instantaneous amplitude (top) and Θ_R (bottom) of the E components of stations LA2 and B12. The data interval begins at 02:38:20 UTC on 18 April 1994.

Analysis of the reduced instantaneous phase calculated using the Hilbert transform is thus a very useful tool for investigating the variations of the frequency of narrowband tremor as a function of time. Because it can be applied to very short intervals, it gives an instantaneous reading of the frequency rather than an average over an interval, allowing observations of very slight and short term changes in the tremor frequency. It is much better suited to studying the frequency of individual narrowband signals than Fourier analysis.

To investigate Θ_R for the higher harmonics, I apply the method to the same interval of the recording at LA2 used for the fundamental. The test frequency for each harmonic, f_n, is $nf_0 = n0.63$ Hz. Although the amplitudes and polarization directions of the various harmonics are very different, the time variation of the frequencies are very similar (Figure 3.13). The intervals with constant slope used in Figure 3.11 can also be recognized in the reduced instantaneous phase of the harmonics. Their slope is exactly n times the slope for the fundamental during the same interval. This means that the harmonics are truly integer multiples of the fundamental.

For an investigation into the physical source of harmonic tremor the intervals between the regions of Θ_R with constant slope are especially interesting. If the frequency of harmonic tremor is a characteristic of the source, frequency changes reflect subtle changes in the physical state variables at or around the source. The changes do not occur suddenly, but gradually over an interval of several seconds or minutes. The frequency changes also take place at different rates.

Figure 3.14 shows the instantaneous amplitude and reduced instantaneous phase for the fundamental at the stations LA2 and B12. Although the instantaneous amplitudes of the E components (Figure 3.14, top) are very different, the similarity of the reduced instantaneous phases (Figure 3.14, bottom) is demonstrated by the fact that the difference, $\Theta_R(\mathrm{BE}) - \Theta_R(\mathrm{LA2E})$, is constant, except where there are jumps of 2π. These two stations are on opposite sides of the volcano, yet during the interval shown, their reduced instantaneous phases indicate that frequency changes are exactly the same at both stations. This is true not only for the stations LA2 and B12, but, aside from jumps of 2π caused by

low SNR, for all other combinations of stations and components, indicating that the frequency of the harmonic tremor and its changes characterize the source.

3.4 Polarization

In earthquake seismology, the polarization of the wave field is used in one of two ways. If the wave type is known, the orientation of the particle motion can be used to determine the direction to the source. On the other hand, if the location of the source is known, the polarization can help distinguish between different types of waves and in addition give some information of the characteristics of the medium such as anisotropy. With four three-component seismic stations and a single source it should be possible to use these insights to determine both the location of the source and the type of wave making up the harmonic tremor wavefield.

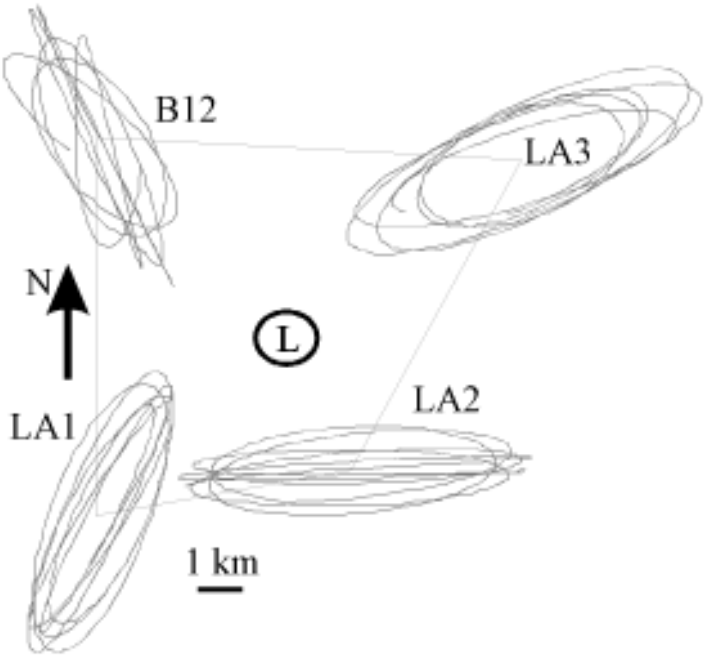

Figure 3.15 Particle motion in the horizontal plane for the fundamental frequency. The diagrams for the same 9.6 s at each station are plotted on a map of the stations of the Lascar network. To isolate the motion for the fundamental, all seismograms were bandpass filtered between 0.5 and 0.9 Hz. The "L" shows the approximate position of Lascar's active crater.

3.4.1 Particle Motion Diagrams

The particle motion of harmonic tremor plotted from the unfiltered ground velocity has no predominant direction of polarization. In contrast, particle motion diagrams become simpler, when the data are filtered using a narrow bandpass filter to select the energy of the individual spectral lines. Figure 3.15 shows the particle motion of the fundamental in the horizontal plane at each of the four stations during the same 9.6 s interval. During subsequent time segments, the particle motion at each station changes only slightly, remaining constant, or nearly so, for intervals much longer than the coherence time [SEIDL and HELLWEG, 1991]. The following discussion will therefore concentrate on the data interval

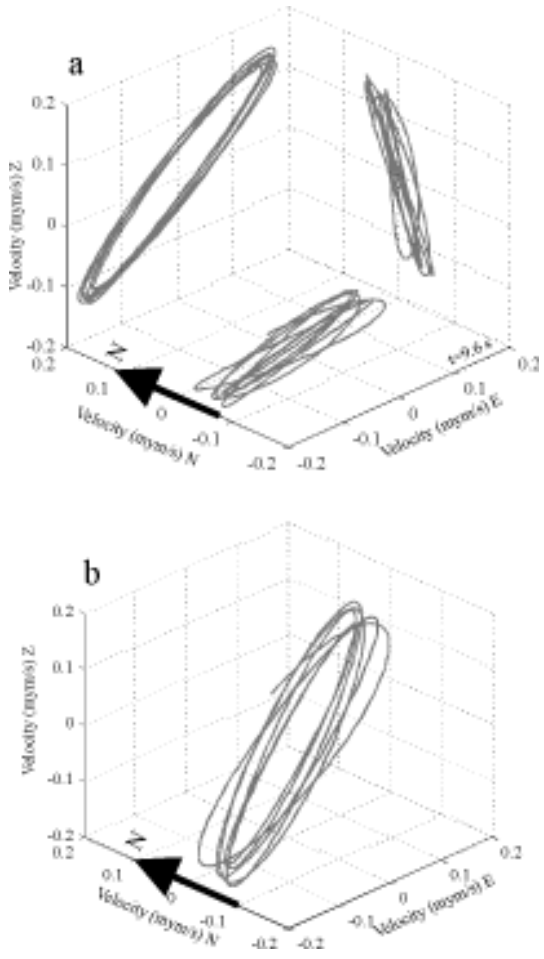

Figure 3.16 Particle motion due to the fundamental frequency at station LA2 for the 9.6 s interval used in Figure 3.15. The data are bandpass filtered between 0.5 and 0.9 Hz. (a) The particle motion is projected onto the Z-N, Z-E and N-E planes. (b) The three-dimensional particle motion is plotted in space.

shown in Figure 3.15 to show general features of the polarization. At station LA2 the horizontal particle motion is relatively stable and almost transverse to the direction to the crater. At B12 and LA3, on the otherhand, the particle motion is nearly radially polarized with respect to the active crater. The particle motion at LA1 is also steady, but neither transverse nor parallel to the crater direction. During the interval shown, the particle motion of the fundamental at the various stations is not consistent with a single wavetype propagating from a single source. Thus, the polarization of the fundamental in the horizontal plane cannot be used to determine the location of the source.

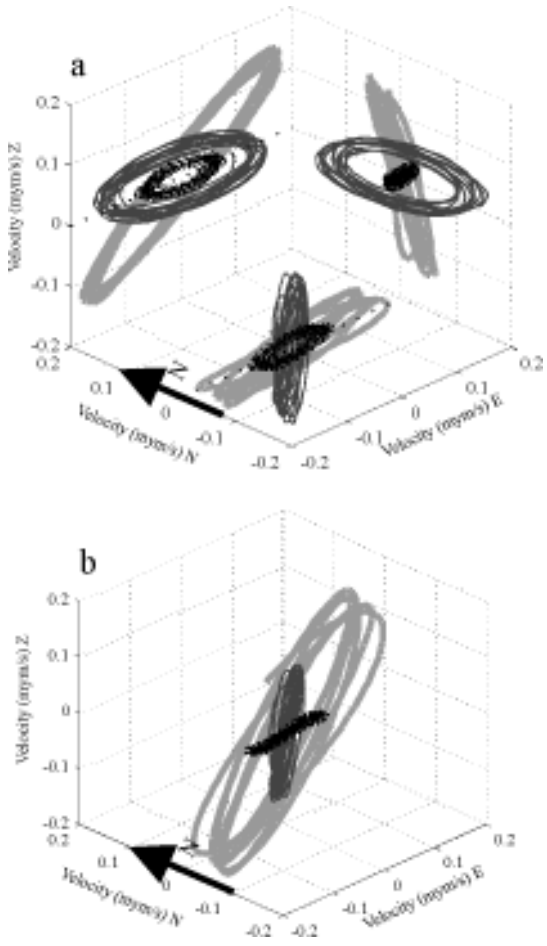

Figure 3.17 Particle motion for the first three harmonics (n =1, 2, 3) at station LA2 for the same interval as Figure 3.15. The data are filtered as follows: fundamental [0.5-0.9] Hz (n =1, light gray), first overtone [0.9-1.5] Hz (n =2, medium gray), second overtone [1.5-2.1] Hz (n =2, black). (a) Particle motion is projected onto the Z-N, Z-E and N-E planes. (b) The three-dimensional particle motion is plotted in space.

This conclusion is reinforced by observations of the particle motion in three-dimensions. To investigate the particle motion in space, I first project it onto the three planes defined by the orientation of the seismometer: the horizontal plane (N-E) and the two vertical planes (Z-N and Z-E). Figure 3.16a gives an example for station LA2. The three-dimensional particle motion diagram is presented in Figure 3.16b.

In Figure 3.17, data for the second and third harmonics (bandpass filters 0.9-1.5 Hz and 1.5-2.1 Hz) are superimposed on that of the fundamental. In the horizontal plane (Figure 3.17a), the fundamental (light gray) and third harmonic (black) appear to have similar orientations. In the three-dimensional representation, however, it is clear that all three spectral lines have completely different polarizations.

The three-dimensional particle motion diagrams for the other stations (Figure 3.18) are similar. At each station, the polarizations for the three harmonics are different. They cannot be interpreted as being produced by a single wave-type generated at a single point source. The same conclusion results from considering the polarization of an individual spectral line at the four stations: There is no simple interpretation in terms of a single source and single wavetype. The relative amplitudes of the lines are also very different at the various stations (Figure 3.18). At station LA2, for example, the fundamental (light gray) has the largest amplitude of the three lines. In contrast, the third harmonic (black) is largest at station LA3, while the second harmonic (medium gray) is largest at B12. This effect may stem from one of two causes: Either the amplitudes of the individual spectral lines are affected differently on their respective paths from source to station, or the radiation of the spectral lines from the source is not isotropic.

3.4.2 Directional Dependence of the Spectral Intensity

In the methods of polarization analysis just described, the polarization is examined separately for each peak in the spectrum. When analysing longer segments of tremor, it is desirable to calculate and display the average polarization for many peaks at the same time. This is possible, if we can calculate the directional dependence of the spectral intensity. To do this, the three component seismograms are rotated in predetermined increments of azimuth and inclination as described by PLEŠINGER et al [1986]. The power spectrum

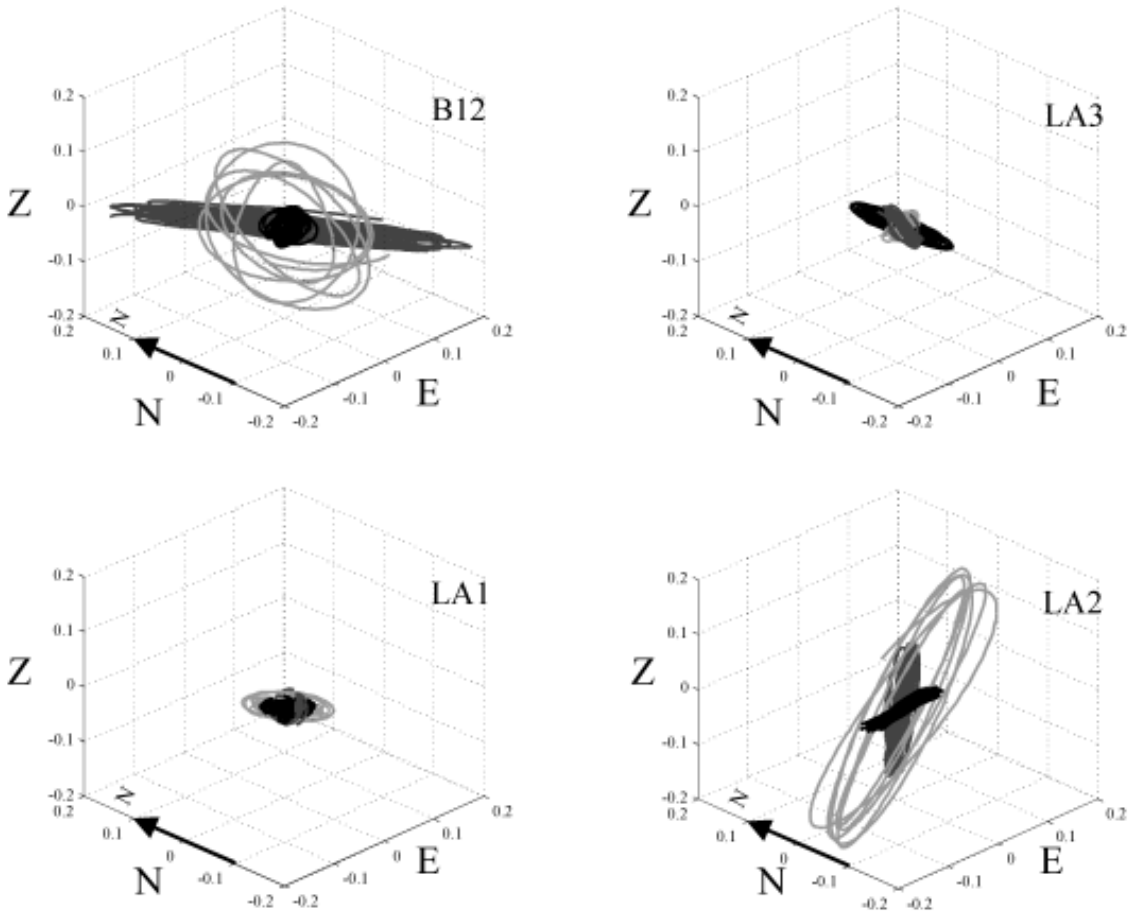

Figure 3.18 The three-dimensional particle motion at each station is plotted in space for the first three harmonics. Data are from the same interval as in Figure 3.15. Colors and filter parameters are as in Figure 3.17. Z, N and E axes give velocity in μm/s.

calculated for each rotated seismogram can then be plotted in different ways. Like all methods using the power spectrum, this method gives an average over the interval analysed. It can only be used to detect the direction of polarization with the highest average spectral intensity for a given frequency.

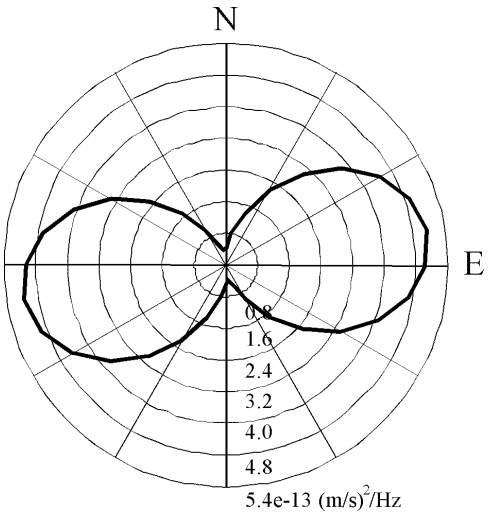

Figure 3.19 Directional dependence of the spectral amplitude of the power at 0.68 Hz in the horizontal plane at station LA2. The spectra are calculated as described for Figure 3.4 from the same 10 minute interval.

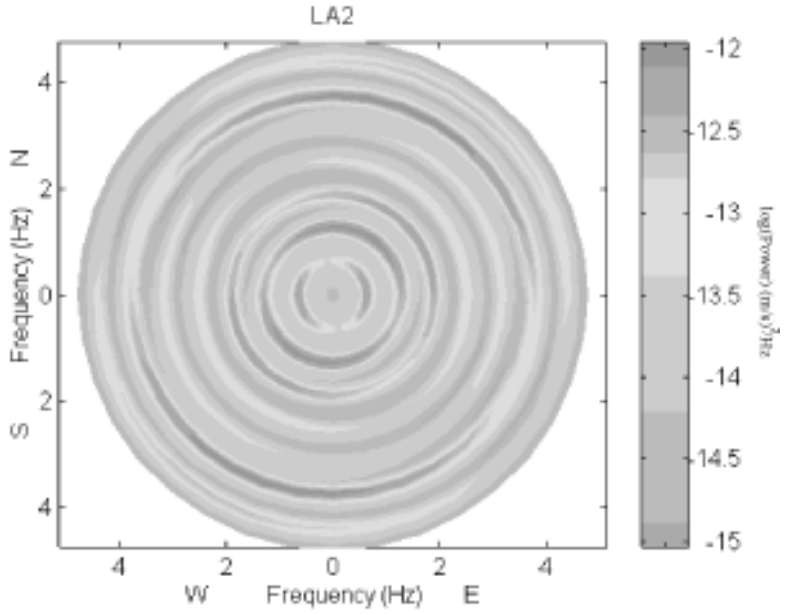

Figure 3.20 Directional dependence of the power spectrum in the horizontal plane at station LA2. The frequency is plotted radially and the spectral amplitude is represented by shading. The spectrum is calculated as described for Figure 3.4 from the same 10 minute interval.

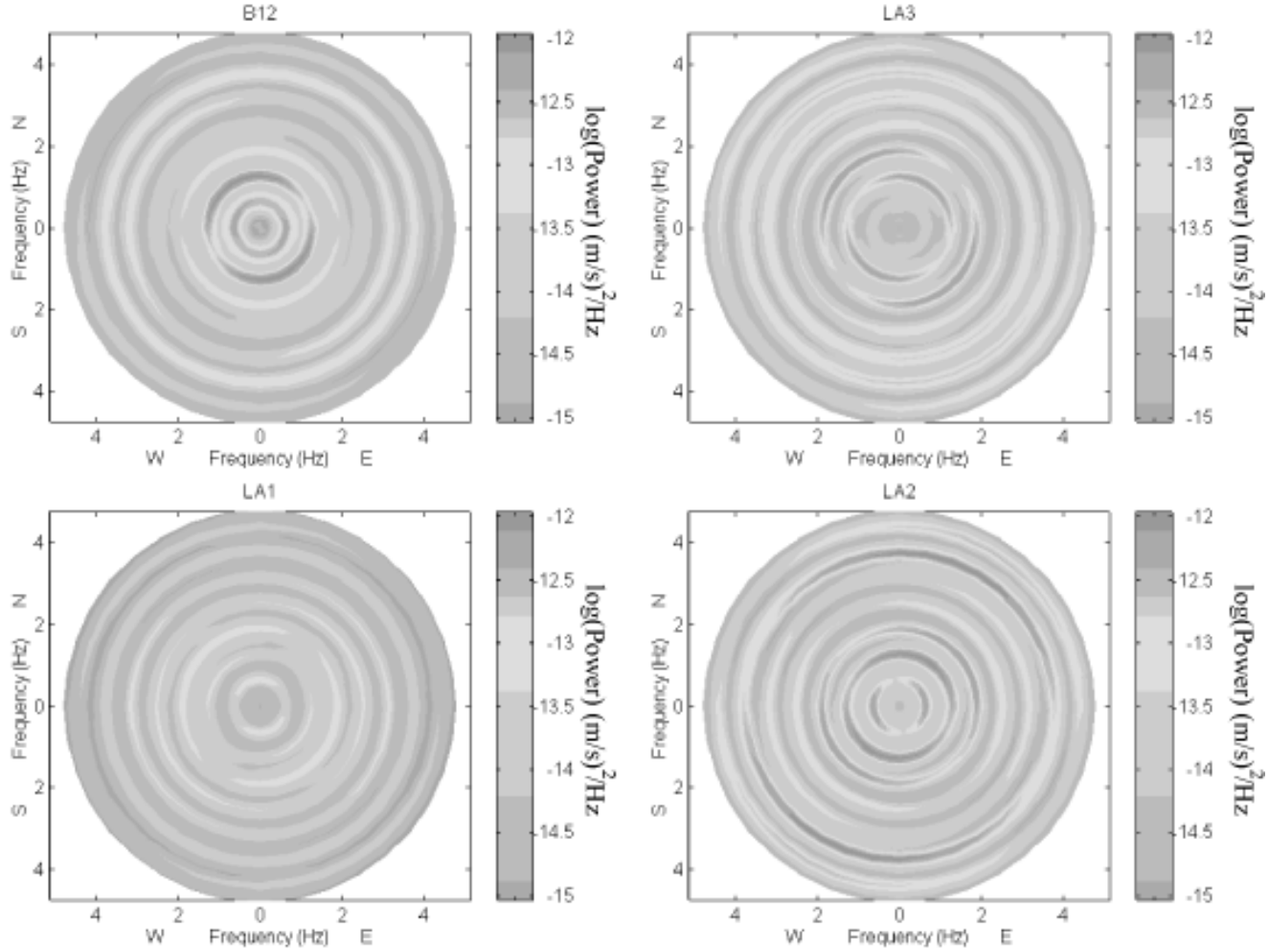

Figure 3.21 Directional dependence of the power spectra in the horizontal plane for the four stations of the Lascar network. The frequency is plotted radially and the spectral amplitude is represented by shading. The spectra are calculated as described for Figure 3.4 from the same 10 minute interval.

The power spectral amplitude for a selected frequency can plotted in the horizontal plane with the angle representing the azimuth and the distance from the origin representing the spectral intensity. In the resulting diagram (Figure 3.19) the direction with the largest amplitude is the direction of the particle motion for which the spectral intensity is largest. This may mean that the amplitude for this direction is exceptionally large for a short period of time, or that the ground moves in this direction most of the time. The minimum amplitude is either a measure for the “background polarization noise” or it may indicate that other polarization directions have a relatively high rate of occurrence.

If the angle represents the azimuth and increasing frequency is plotted in the radial direction, the spectral intensity as a function of azimuth and frequency can be indicated by shading. Figure 3.20 shows the primary polarization directions for the first seven peaks at station LA2. This figure confirms the observation in Section 3.4.1 that the polarization is different for different peaks. In Figure 3.21, the directional dependence of the spectral intensity as a function of frequency is plotted for all four stations. None of the spectral peaks has a polarization field which permits a unique identification of its wavetype if the source of the seismic waves is in or near the crater.

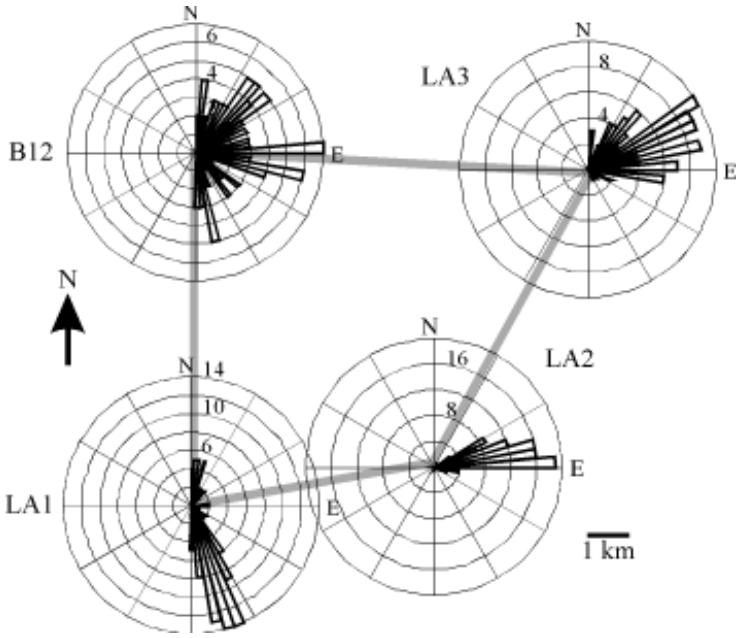

Figure 3.22 Horizontal polarization rosettes for all stations for the fundamental. The rosettes are plotted on a diagram of the Lascar network. The data are taken from the interval described in Figure 3.4, and were filtered using a bandpass filter [0.5-0.9] Hz.

3.4.3 Polarization Rosettes and Polarograms

With the methods described in Section 3.4.1 the polarization can only be studied for short intervals, while Section 3.4.2 shows the mean polarization, but only in two dimensions. An extension of the polarization rosette method [Seidl and Hellweg, 1992] to histograms offer an alternative means of studying the three dimensional polarization of longer intervals. If three component recordings are bandpass filtered to separate the energy of the individual spectral lines, the resulting seismograms are nearly sinusoidal. The three-dimensional particle motion diagrams for short intervals are ellipsoids (Figure 3.16). The major axis of a particle motion ellipsoid for a particular time interval, and thus its polarization direction, can be calculated using the covariance of the three filtered seismograms [Matsumura, 1981, Kanasewich, 1981]. The polarization direction is defined as the direction of the eigenvector which corresponds to the largest eigenvalue of the covariance matrix.

Seidl and Hellweg [1992] show the results of such calculations as an azimuthally plotted histogram, or rosette, of the azimuths of the largest eigenvectors. The most common directions of polarization for the fundamental recorded at the four stations during a 10 minute interval, shown in Figure 3.22, agree with the particle motion for the short intervals shown in Figure 3.15.

The third component of motion is lost in this representation, however. Figure 3.22 gives no information about the inclination of the particle motion with respect to the horizontal plane. The representation of inclination originally chosen by Seidl and Hellweg [1992] — also a histogram in an arbitrarily selected vertical plane — can easily be misinterpreted. To avoid this, it is better to plot the azimuth and inclination explicitly in a polarogram. Figure 3.23 shows polarograms for the first six harmonics recorded at station LA2. The polarization of the fundamental at station LA2 (Figure 3.23, f1) has a sharp peak at 70° E azimuth and an inclination of 40° from the horizontal. For the second harmonic (Figure 3.23, f2), the method distinguishes two horizontal polarization directions, each with a unique inclination. Thus, the particle motion due to the second harmonic at the station LA2 has two directions of predominant polarization with different azimuths and inclinations. The higher order harmonics (Figure 3.23, lower four diagrams) also differ in their polarization. The polarization

differences among the harmonics observed during a short interval are also apparent in this analysis over a longer period.

The results from the polarization of a short data interval from the individual stations and the various harmonic frequencies presented in Section 3.4.1 are confirmed for longer intervals using

Table 3 -- Polarization Directions

Station	Azimuth from N	Inclination from H
B12	90°, 60°	0°, 15°
LA1	160°, 10°	10°, -5°
LA2	70°	40°
LA3	70°, 30°	5° ,5°

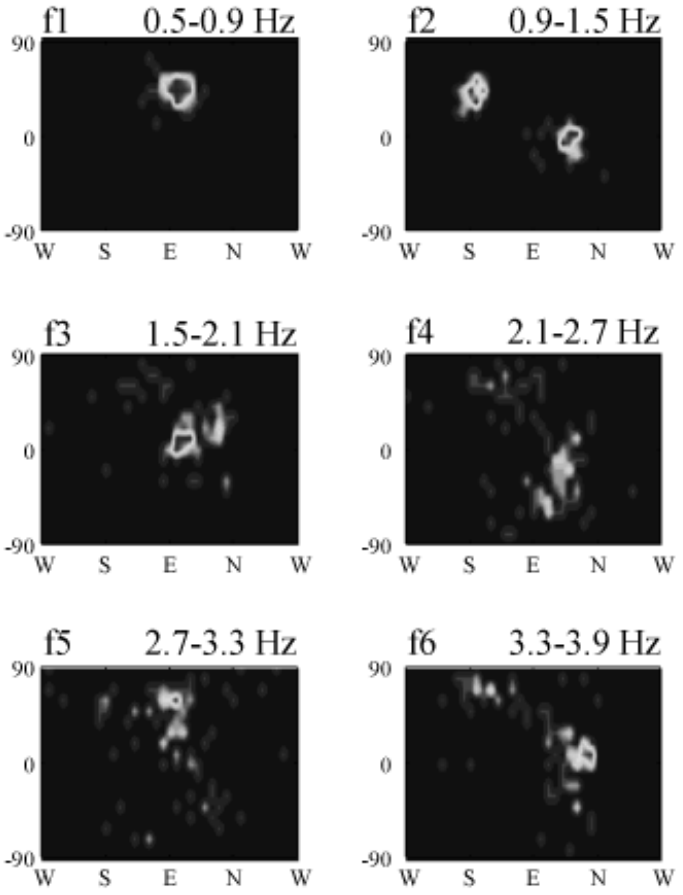

Figure 3.23 Polarograms for the first six harmonics at LA2 taken from the same interval as Figure 3.4. The horizontal axis gives the azimuth of the particle motion while the vertical axis gives its inclination from horizontal. The shading gives the number of times that a polarization ellipsoid occurs with the given orientation (N>6 dark centers). The filter corner frequencies are given on the respective plots.

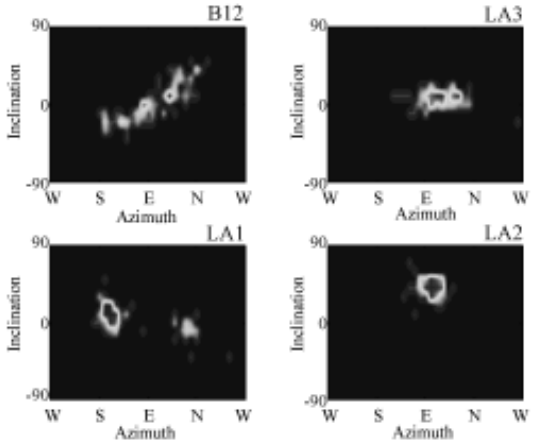

Figure 3.24 Polarograms of the four stations for the fundamental, f1: 0.5-0.9 Hz.

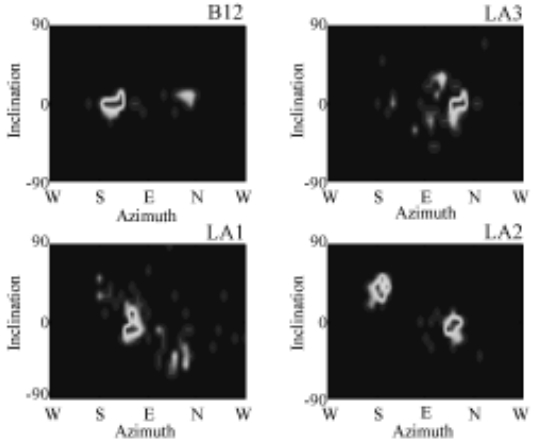

Figure 3.25 Polarograms of the four stations for the first overtone, f2: 0.9-1.5 Hz.

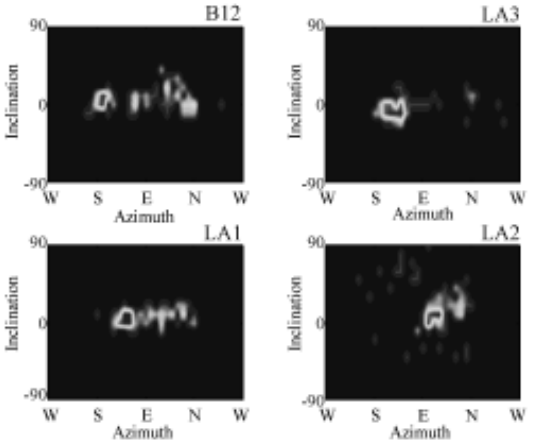

Figure 3.26 Polarograms of the four stations for the second overtone, f3: 1.5-2.1 Hz.

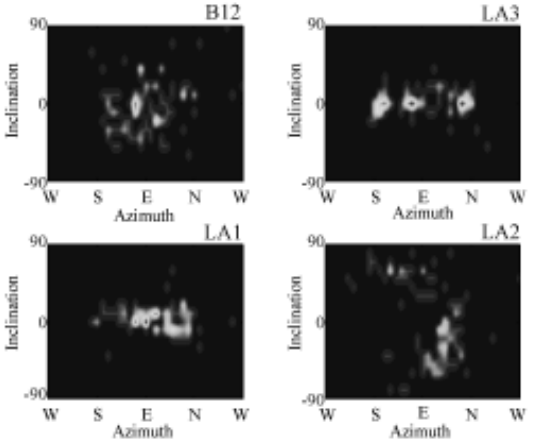

Figure 3.27 Polarograms of the four stations for the third overtone, f4: 2.1-2.7 Hz.

polarograms. Figures 3.24 through 3.27 show polarograms for the fundamental through the fourth harmonic at the four stations. The primary polarization directions for the fundamental are listed in Table 3 with the azimuth given in degrees from north (N) and the inclination in degrees from horizontal (H). None of the figures is consistent with a wavefield from a single source, for example the active crater, consisting of a single type of waves.

3.5 Summary of Observations and their Implications for Harmonic Tremor

The seismogram characteristic which is most consistent across components and stations is the fundamental frequency of the harmonic tremor. As demonstrated by both the phasor-walkout diagrams and plots of the reduced instantaneous phase, frequency changes occur at the same times and at the same rates at all stations. The frequencies of the integer harmonics also follow changes in the frequency of the fundamental exactly, $f_n(t) = nf_1(t)$ (where n = 1,2,3...). At times, more than 25 peaks can be observed in the spectrograms.

Peaks in a seismic spectrum are often attributed to path or site effects [Seidl et al, 1981 and Chouet, 1996]. However, since the frequencies are the same for all components at all stations, but the geologic conditions at the stations are different (Table 1), local conditions or path effects probably do not cause the many frequency peaks observed in Lascar's harmonic tremor. In addition, the influences of path and site cannot explain the changes in the fundamental frequency and the overtones that occur at the same time at all stations. The fundamental frequency must therefore be a characteristic of the source. The presence of energy at the frequencies of the harmonics at all stations indicates that these peaks are also generated at or near the source.

When the spectrum of volcanic tremor has more than one peak with at high signal-to-noise ratio, the seismic waves producing the peaks are usually attributed to different sources [Chouet, 1996]. This is unlikely to be the case for the harmonic spectrum of Lascar's volcanic tremor, because there are so many overtones and their frequencies follow the frequency of the fundamental exactly. Harmonic spectra such as this are observed when the amplitude of the source is is limited by non-linear effects.

In most seismological studies using three component data, the polarization of wavegroups at several stations can be used to determine whether the arriving signals are P-, S- or surface waves and the probable direction to the source. Despite several different attempts at polarization analysis, such considerations cannot successfully be applied to harmonic tremor. At a given station, the polarization direction is different for each of the harmonics. In addition, the polarization for a specific frequency, as measured at the four stations of the Lascar network cannot be reconciled with a single wavetype from a single point source. On the otherhand, the polarization at each of the stations remains relatively constant over long intervals. As demonstrated in the polarograms, each harmonic produces only one or at most two polarization directions at each station. Although the particle motion cannot be used to determine the direction to the source, its long term stability indicates that the source remains in the same place for an extended time

The apparently complicated polarization of Lascar's harmonic tremor may be due to unusual radiation patterns of a source that can be described neither an explosive point source nor as the double couple familiar from earthquake seismology. However, the polarization of the harmonic tremor wavefield is also affected during propagation in the complicated medium that is the volcanic edifice.